Ion beam triangulation based on electron detection for studies on the structure of 1 ML Mn on Cu(001)

2009 J. Phys.: Condens. Matter 21 134001

(http://iopscience.iop.org/0953-8984/21/13/134001)

J. Phys.: Condens. Matter **21** (2009) 134001 (6pp) doi:10.1088/0953-8984/21/13/134001

Ion beam triangulation based on electron detection for studies on the structure of 1 ML Mn on Cu(001)

T Bernhard, J Seifert and H Winter

Institut für Physik der Humboldt-Universität zu Berlin, Newtonstraße 15, D-12489 Berlin-Adlershof, Germany

Received 8 October 2008, in final form 5 November 2008
Published 12 March 2009
Online at stacks.iop.org/JPhysCM/21/134001

Abstract
Recent developments in studies on the structure of surfaces based on ion beam triangulation are discussed. We will outline recent experimental progress in the application of this method, which is closely related to the detection of the number of emitted electrons per incident ion during scattering under surface channeling conditions. Key features are the pronounced change of electron emission for the projectile beam aligned along a low index crystallographic direction in the surface plane ('axial surface channeling') and the interpretation of data in terms of classical trajectory computer simulations. As a representative example we will discuss here studies on the structure of the low temperature c(8 × 2) Mn/Cu(001) phase.

(Some figures in this article are in colour only in the electronic version)

1. Introduction

The structure of surfaces plays an important role in fundamental research and technological application, since it affects the electronic, magnetic or chemical properties of the interface in a decisive manner. Reconstruction phenomena in the surface region can be complex so that studies on the detailed geometrical structure of a solid surface are still a challenging task. A fair number of powerful experimental as well as theoretical methods have been developed in recent decades which allows one to study the reconstruction of the surface of clean and adsorbate covered targets or of thin films. From the experimental side these techniques are based on the diffraction of low (LEED) (Heinz *et al* 2000) and high energy electrons (RHEED) (Mahan *et al* 1990), on diffraction of photoelectrons (PhD) (Woodruff and Bradshaw 1994), scattering of photons (SXRD, NEXAFS) (Stöhr 1992) or, in particular, on scanning tunneling microscopy (STM) (Binnig and Rohrer 1982). On the theoretical side methods based on the density functional concept (DFT) (Lang and Kohn 1970) play a pivotal role. The interpretation of experimental data can be quite intricate, and the experience with studies on the surface structure over the years has shown that it is generally difficult to end up with a clear cut solution for a structural model on the basis of a single spectroscopic method.

Recently, we have introduced a new variant of the ion beam triangulation (IBT) technique (Pfandzelter *et al* 2003a) for surface structure analysis where fast atoms or ions with energies of typically some 10 keV are scattered under a grazing angle of incidence from a target surface in the regime of surface channeling (Winter 2002). A key feature for the application of ion scattering in a triangulation technique is the observation that the kinetic emission of target electrons induced by the fast projectiles shows a pronounced dependence on the azimuthal settings of the target surface (Winter *et al* 2004). Whenever the direction of the incident projectile beam coincides with a low indexed direction of a monocrystalline surface or of a complex superstructure, the projectiles are scattered in the regime of axial surface channeling. Then the symmetry for the scattering from the surface is changed from a planar type for 'random' azimuthal orientation to an axial one with respect to atomic strings. The substantial change of trajectories for the transition from planar to axial channeling is accompanied with a modification of electron emission, since under axial channeling projectiles may reach domains of higher electron density within the axial channels or may even penetrate into the bulk.

In this paper we will focus on recent developments in the application of IBT for studies on surface structure and will discuss in detail as a representative example investigations on the c(8 × 2) Mn/Cu(001) structure. We will compare different methods for the detection of electron emission during ion impact and their benefits for the application in IBT. It

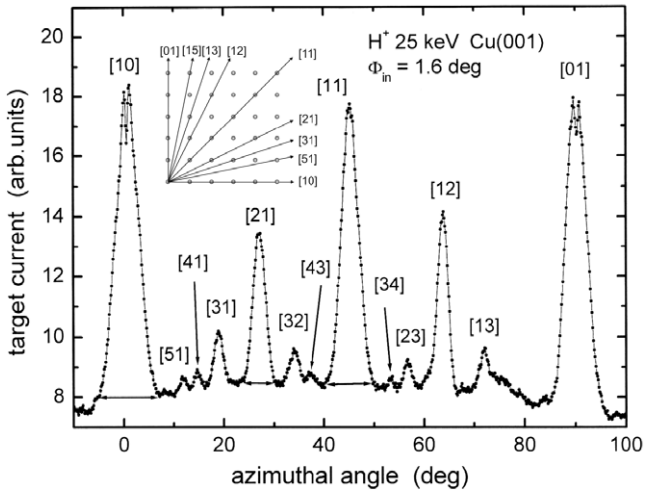

Figure 1. Uncompensated target current as a function of azimuthal angle of rotation for scattering of 29 keV protons from Cu(001) under $\Phi_{in} = 1.6°$. Inset: sketch of surface structure for Cu(001) surface and resulting axial channels.

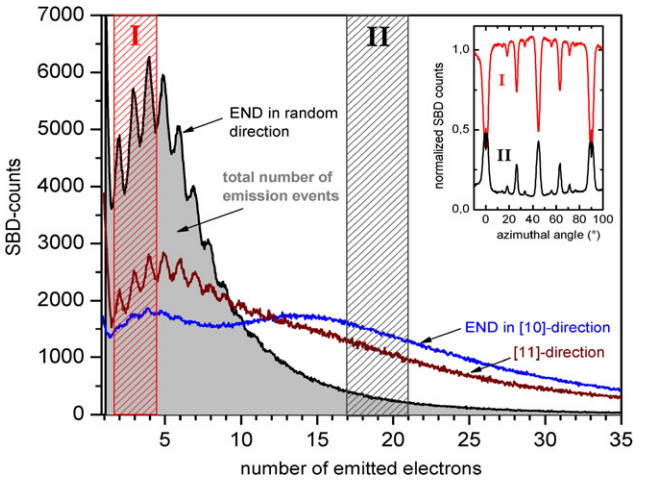

Figure 2. (Color online) Pulse height distributions of SBD for scattering of 25 keV He^0 atoms from Cu(001) under $\Phi_{in} = 1.6°$ and random azimuthal alignment with respect to incident beam (black curve), alignment along [10] (blue curve) and alignment along [11] (red curve). The hatched areas denote settings of discriminator levels: I = detection of 2–4 electrons, II = detection of 17–21 electrons. Inset: IBT curves for low (red curve) and high (black curve) numbers of emitted electrons.

turns out that the detection of the number of electrons emitted per incident projectile is a particularly interesting variant of IBT which makes this technique very attractive for studies on surface structures. The number of emitted electrons as a function of the azimuthal angle of rotation of the target surface can be analyzed in terms of classical trajectory computer simulations which provide detailed tests of structural models.

2. Experimental methods

In ion beam triangulation (IBT) studies a target surface with a defined geometrical structure is bombarded under UHV conditions (base pressure some 10^{-11} mbar) with a well collimated beam of fast ions/atom with kinetic energies of typically some 10 keV. The projectiles are scattered under a grazing angle of incidence of about 1° from the surface in the regime of surface channeling (Winter 2002, Niehus *et al* 1993). The simplest way to monitor electron emission is by recording the (uncompensated) target current (Pfandzelter *et al* 2003a) during projectile impact which is induced by the charge exchange of scattered particles and, in particular, by emission of electrons. Then IBT can be performed by recording the target current during the azimuthal rotation of the target surface. In figure 1 we show as an example data for the scattering of 25 keV H^+ ions from a Cu(001) surface under a grazing angle of incidence $\Phi_{in} = 1.6°$ (Pfandzelter *et al* 2003a). The curve reflects the symmetry of the (001) face of an fcc crystal with prominent peaks for the [10], [01] and [11] directions of the 2D surface lattice. The peaks can be understood by enhanced electron emission for axial channeling where the loss of target electrons mimics an enhanced target current. For the prominent peaks the current is enhanced by a factor of 2 and directions of higher indices up to [51] can be identified in the spectra.

Recently, an alternative scheme of detection was proposed which is based on the number of electrons emitted per ion/atom impact on the target surface (Bernhard *et al* 2005). These numbers are obtained by means of a surface barrier detector (SBD) biased to a high voltage of some 10 keV (typically 25 keV) so that electrons emitted from the surface are accelerated onto the detector entrance area and produce in the barrier region electron–hole pairs proportional in number to the energy of the incident electrons. Since the pair creation in the SBD induced by electrons emitted in a single collision event lead to a pile up of the output pulses from the detector, the pulse height of the SBD is directly proportional to the number of emitted electrons (Aumayr *et al* 1991). Pulse height spectra (related to electron numbers) result in electron number distributions (END) which are displayed for scattering of H^0 atoms from a Cu(001) surface in figure 2 for a random azimuth and for the [10] and [11] directions. For random orientation the pulse height spectra reveal discrete peaks which can be attributed to specific numbers of emitted electrons. A key feature for IBT is the finding that, for scattering along the low indexed azimuths, the (normalized) spectra are shifted toward higher electron numbers, i.e. events with a higher number of emitted electrons are more probable. Then triangulation can be performed by selection of low electron number or high electron number events where the total number of emission events is constant and can be used for a very efficient normalization of data.

In the inset of figure 2 we show two IBT curves recorded for the settings of the discriminator levels equivalent to the detection of 2–4 electrons (red curve) and to about 15–20 electrons (black curve). For the detection of low electron numbers a dip structure is observed (shift of electron number spectra towards higher numbers for axial channeling and a reduction of events with low numbers), whereas events for high electron numbers are increased and the curve shows peaks for axial surface channeling.

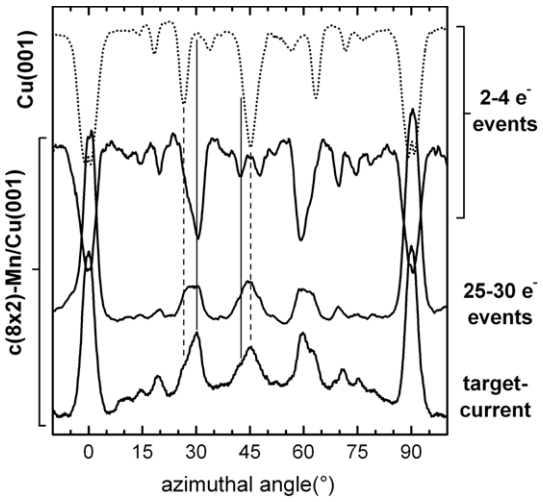

Figure 3. IBT signal as a function of azimuthal angle. Dotted curve on top: signal for clean Cu(001) and detection of 2–4 electrons, lower curves: signal for c(8 × 2)-Mn/Cu(001).

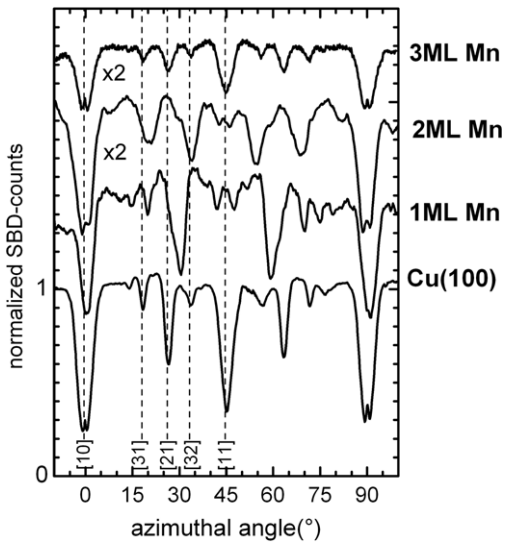

Figure 4. SBD signal (2–4 electrons detected) as a function of azimuthal angle for clean Cu(100) and coverage of 1 ML Mn, 2 ML Mn and 3 ML Mn.

In figure 3 we display IBT curves detected with the electron number detector for clean Cu(001) (dotted curve) and for a 1 ML Mn film on Cu(001) (solid curves). In the upper solid curve the discriminator levels are adjusted to the detection of 2–4 electrons, while in the middle curve events related to the emission of 25–30 electrons are selected. In the bottom curve the target current is plotted (Bernhard *et al* 2003). All curves show a number of dips or peaks which can be related to low indexed axial channels for the Mn superstructure formed on the Cu(001) substrate. We note that the peaks for the high electron number events and for the target current do not only represent the structure of the film, but also show signatures of the Cu substrate. In figure 4 we present IBT studies for the growth of ultrathin films of Mn on Cu(001). The data reveal the transition from a (1 × 1) structure for the clean metal surface, to a c(8 × 2) superstructure for a coverage of 1 ML Mn and c(12 × 8) for 2 ML Mn (Pfandzelter *et al* 2003b). The substantial reduction of peak heights for the Mn films can be attributed to a rougher surface compared to the clean substrate.

From the comparison of data obtained for the 1 ML Mn film by the two different methods of detection of electron emission follow a number of interesting features which favor the method based on recording the electron number distributions.

(1) The emission of low numbers of electrons is closely related to interaction processes located in front of the topmost surface layer. For penetration of projectiles into the bulk, enhanced electron densities and longer trajectories lead to clearly larger total electron yields. As a consequence, monitoring IBT curves for low electron numbers selects emission events in the selvedge of the surface and provides a clear cut selection of data to the structure of the topmost surface layer only. This is an important issue for the interpretation of data in terms of classical trajectory computer simulations. A comparison of the two curves for substrate (dotted curve) and 1 ML Mn film (upper solid curve) in figure 3 reveals drastic changes in the dip structures of the IBT curves which demonstrates the extreme sensitivity of the method to the structure of the topmost surface layer. A prominent example in this respect is the complete disappearance of the dip at an azimuth of 45° for the diagonal in the square lattice of Cu(001) owing to the structural change to a quasi-hexagonal arrangement of Mn atoms.

(2) Total electron yields for kinetic emission induced by ion/atom impact are higher for a rough surface compared to a flat target which can be attributed to binary collisions with individual surface atoms. By selecting events related to a low number of emitted electrons, the influence of surface roughness and steps on the IBT curve can be substantially reduced and appear in an overall enhanced constant background signal only. This can be seen in the data for a higher coverage of 3 ML shown in figure 4 where the transition from the c(12 × 8) to the p(1 × 1) can be clearly identified.

(3) The number of light ions/atoms (H, He) impinging on the target for the detection of electrons with a biased SBD is extremely low. Since the total electron yields are sufficiently high, each projectile produces at least one electron, and since the electron detection efficiency is close to 1, each projectile is counted. The maximum count rate of the SBD is about 10^4, which corresponds to a current of incident ions of typically fA. This flux of light projectiles is so low that radiation damage even for sensible surface structures can be neglected.

(4) Since each projectile is counted, the total number of counts is not changed for the transition from planar to axial channeling (only the electron number spectra are shifted to higher numbers) so that the total number is an excellent tool for the normalization of data. It turns out that this procedure eliminates to a major extent effects owing to fluctuations of the projectile beam.

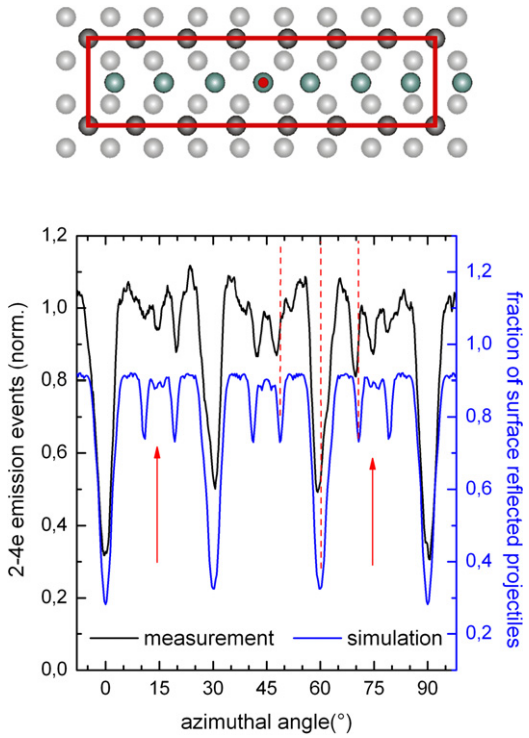

Figure 5. (Color online) Upper panel: structural model for c(8 × 2)-Mn/Cu(001) from Gauthier *et al* (1994). Lower panel: SBD counts (2–4 electrons detected) for scattering of 29 keV H^0 atoms scattered from 1 ML Mn on Cu(001) under $\Phi_{in} = 1.6°$ (black curve) and results from computer simulations (blue curve).

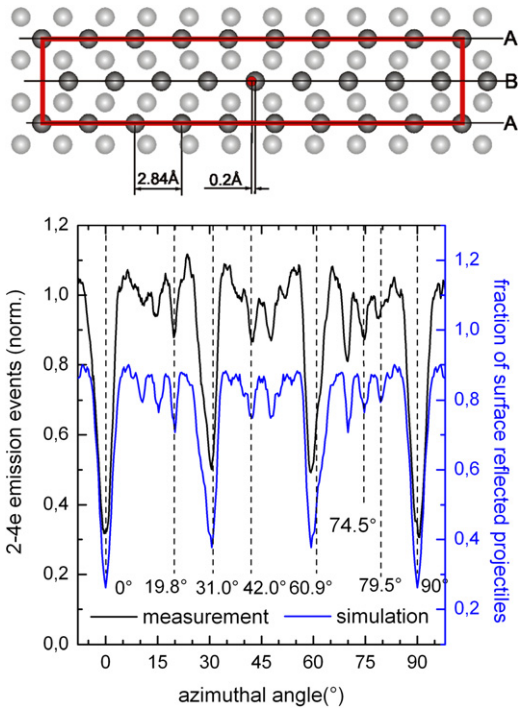

Figure 6. (Color online) Upper panel: revised structural model. Lower panel: SBD counts (2–4 electrons detected) for scattering of 29 keV H^0 atoms scattered from 1 ML Mn on Cu(001) under $\Phi_{in} = 1.6°$ (black curve) and results from computer simulations based on the revised structural model proposed in this work (blue curve).

(5) The method can be applied *in situ* and without delay after the preparation of the target surface of the ultrathin film. The recording of IBT curves can be performed in typical times of some minutes so that, for example, modifications of the surface structure owing to adsorption of impurity atoms can be widely excluded. In addition, investigations over a wide range of target temperatures are feasible *in situ* with the present set-up.

3. Results and discussion of studies on the c(8 × 2)-Mn/Cu(001) phase

For the growth of ultrathin Mn films on Cu(001) Flores and coworkers (1992) proposed a phase diagram for deposition temperature and Mn coverage. A variety of different superstructures are stated ranging from a c(8 × 2) structure for low temperatures and a thickness of 1 ML and a c(12 × 8) structure for 2 ML. At higher temperatures, one finds c(2 × 2) and p2gg(4 × 2) superstructures, and for a coverage larger than about 2 ML Mn atoms occupy (1 × 1) positions with respect to the substrate (see data for 3 ML Mn in figure 4). In this work we concentrate on the low temperature phase at an Mn film thickness of 1 ML, which was assigned to a c(8 × 2) structure. This structure has been studied in terms of a detailed *I*–*V* LEED analysis by Gauthier *et al* (1994), and the structural model proposed by these authors is sketched in the upper panel of figure 5. A key feature of this model is a quasi-hexagonal arrangement of Mn atoms along the densely packed [10] rows where strings of 7 Mn atoms are relaxed to 8 Cu atoms of the substrate, i.e. the distance between nearest Mn neighbors is $d_{Mn[10]} = 8/7 \times 2.556$ Å $= 2.92$ Å, comprising a pronounced corrugation.

In the lower panel of figure 5 we show the IBT curve for 1 ML of Mn grown at $T = 200$ K at a rate of 0.007 ML s^{-1} (black curve). The blue curve in figure 5 represents results from computer simulations for the structural model from Gauthier *et al* (1994) (cf upper panel of figure 5). In these calculations the trajectories of projectiles are obtained from Newton's law and interatomic potentials as proposed by O'Connor and Biersack (O'Connor and Biersack 1986). These potentials are based on the Thomas–Fermi model for atoms and are characterized by a modified screening length for the Moliere potential (Moliére 1947). Lattice vibrations are taken into account in terms of the Debye model for a frozen lattice and uncorrelated oscillations. Here we employ a 'penetration criterion' for the separation of events related to a low or high number of emitted electrons. The basic feature of this criterion is the distance of closest approach for trajectories during scattering events. Whenever projectiles reach a region slightly below the topmost layer of surface atoms, we assume that such trajectories lead to an enhanced emission of electrons. It turns out that this simple criterion works fairly well for systems with surface atoms with comparable atomic numbers. In the simulation procedure the number of events for penetration and no penetration are counted for randomly distributed initial

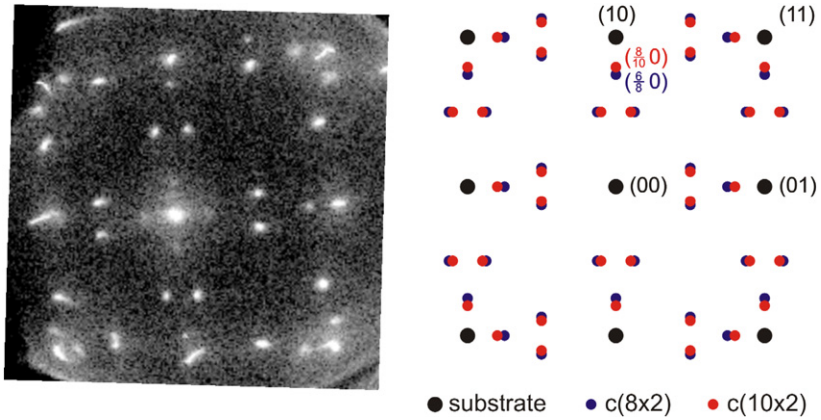

Figure 7. LEED pattern recorded by SPALEED system with 50 eV electrons for 1 ML Mn film grown at 200 K on Cu(001) (left panel) and sketch for structure of LEED pattern (right panel).

starting points of trajectories with respect to the unit cell at fixed azimuthal orientations of the target surface.

We reveal that the gross structures of the experimental IBT curve are reasonably well reproduced for the simulations using the structural model by Gauthier *et al* (1994): however, in more detail specific deviations between simulations and experiment are present. In general, slight shifts for several dips by about 1° are found and the smaller dips between 10° and 20° as well as 70° to 80° are not in accord with the experiment. In particular, at an azimuth of $\Theta = 74.5°$ we observe in the experiment a dip which is missing in the simulations, whereas the size of the dip at $\Theta = 79.5°$ is overestimated in the simulations. We therefore conclude that slight shifts of the mean distances between atoms along the strings forming the unit cell are needed, i.e. the size of the unit cell has to be changed.

In the upper panel of figure 6 we show a modified structural model for the low temperature phase of 1 ML Mn on Cu(001). The model corresponds to a c(10 × 2) unit cell where nine Mn atoms are positioned along ten atoms of the Cu substrate so that the distance between adjacent Mn atoms amounts to $d_{\mathrm{Mn}[10]} = 10/9 \times 2.556$ Å $= 2.84$ Å. In addition, we suggest a lateral shift of the positions of Mn atoms of adjacent strings by 0.2 Å in order to obtain better agreement with the IBT curves for azimuthal angles between 10° and 20°. With this model we find near-perfect agreement of our simulations with the experiment and conclude that the lateral positions of the low temperature 1 ML Mn/Cu(001) phase has to be close to the positions proposed here. From the effect of a variation of the atom positions on the simulated IBT curves we conclude that the accuracy of these positions is about 0.05 Å. In this respect we have to stress that IBT has a poorer sensitivity on the vertical and lower layer positions, since these atom positions have less effect on projectile trajectories and the resulting emission of electrons. This feature of IBT is, to some extent, complementary to the properties of the *I*–*V* LEED method where the figure of merit, expressed in the Pendry *R* factor, turns out to be exceedingly sensitive to vertical positions of lattice atoms, whereas lateral shifts of atomic positions show a weak dependence for *R* only. Therefore we propose the combination of IBT and *I*–*V* LEED as a very powerful tool for investigations on the detailed real space structure of surface.

Finally we mention that the LEED pattern recorded by us with a SPALEED system (Omicron Nanotechnology, Taunusstein, Germany) directly after IBT studies as shown in figure 7 can be interpreted in terms of our revised structural model. The LEED spots show a pattern which cannot unequivocally be ascribed to a c(8 × 2) or c(10 × 2) superstructure. However, the (6/8 0) spot of a c(8×2) pattern is closer to the (1 0) spot which points towards a (8/10 0) position of a c(10 × 2) structure. The reduced Mn distance along [10] directions leads to an enhanced areal density compared to the c(8 × 2) superstructure model, but is still 11% lower than the density of the hexagonal γ-Mn(111) surface. This differs from other quasi-hexagonal films on fcc(001) metal surfaces, where the observed areal density is close to the corresponding (111) surface, as pointed out by Gauthier *et al* (1994).

Acknowledgments

We are particularly grateful to Professor K Heinz and Dr L Hammer (Universität Erlangen) for many fruitful discussions and their continuous encouragement and support during the development of the IBT method. This work was supported by the Deutsche Forschungsgemeinschaft under contract Wi 1336. We thank G Lindenberg, K Maass, Dr R Pfandzelter and U Linke (Jülich) for their assistance in the preparation of the experiments.

References

Aumayr F, Lakits G and Winter H 1991 *Appl. Surf. Sci.* **47** 139
Bernhard T, Baron M, Gruyters M and Winter H 2005 *Phys. Rev. Lett.* **95** 087601
Bernhard T, Pfandzelter R and Winter H 2003 *Surf. Sci.* **543** 36
Binnig G and Rohrer H 1982 *Phys. Rev. Lett.* **49** 57
Flores T, Hansen M and Wuttig M 1992 *Surf. Sci.* **279** 251
Gauthier Y, Poensgen M and Wuttig M 1994 *Surf. Sci.* **303** 36
Heinz K, Starke U and Bernhardt J 2000 *Prog. Surf. Sci.* **64** 163
Lang N D and Kohn W 1970 *Phys. Rev.* B **1** 4555
Mahan J E, Geib K M, Robinson G Y and Long R G 1990 *J. Vac. Sci. Technol.* A **8** 3692
Moliére G 1947 *Z. Naturf.* a **2** 133
Niehus H, Heiland W and Taglauer E 1993 *Surf. Sci. Rep.* **17** 213

O'Connor J D and Biersack J P 1986 *Nucl. Instrum. Methods* B **15** 14
Pfandzelter R, Bernhard T and Winter H 2003a *Phys. Rev. Lett.* **90** 036102
Pfandzelter R, Bernhard T and Winter H 2003b *Surf. Rev. Lett.* **10** 399
Stöhr J 1992 *NEXAFS Spectroscopy* (*Springer Series in Surface Sciences*) (Berlin: Springer)
Winter H 2002 *Phys. Rep.* **367** 387
Winter H, Maass K, Lederer S, Winter H P and Aumayr F 2004 *Phys. Rev.* **69** 054110
Woodruff D P and Bradshaw A M 1994 *Rep. Prog. Phys.* **57** 1029